

Galaxies, Cosmology and Dark Matter



Lecture given by
Ralf Bender
USM

Script by:
Christine Botzler, Armin Gabasch,
Georg Feulner, Jan Snigula

Summer semester 2000


Chapter 7

Elliptical Galaxies

7.1 Overview

- Until the late 1970's elliptical galaxies remained mostly unknown territory. Their surface brightness profiles and colours had been measured, but nothing was known about their intrinsic dynamics and only little about their intrinsic stellar populations. Therefore the general paradigm was that ellipticals
 - were kind of disk-less bulges (because of similar density profiles),
 - were flattened by rotation (nobody thought of anisotropy!),
 - did not contain significant amounts of gas, and
 - were composed of old stars only.

- Between 1977 and 1992 it turned out that nearly all of these (premature) conclusions are not correct:
 - 1975/77/78: massive** elliptical galaxies show only little rotation (Bertola, Capaccioli, Illingworth), they must be supported by **anisotropic velocity dispersion** (Binney).
 - 1978/85:** elliptical galaxies contain up to $10^9 M_{\odot}$ **hot gas** of about 10^7 K (Einstein satellite, Forman, Jones, Tucker)
 - 1988:** a significant fraction of **massive** elliptical galaxies contains kinematically decoupled (e.g. **counter-rotating**) centers (Bender, Franx and Illingworth, Jedrzejewski and Schechter)
 - 1988/89:** many elliptical galaxies contain **weak stellar disks**, not previously detected (Bender et al., Rix and White)
 - 1984/92:** it is indicated that the stars in ellipticals are not genuinely old and that especially lower luminosity ellipticals may contain stars that are "only" 5 Gyr old (Faber, Burstein, O'Connell, Schweizer)

 **today:** many questions about the formation and the evolution of elliptical galaxies are still under intense study:

- what is the star formation history of ellipticals?
- when is most of their mass assembled and how (merger history)?
- does the age depend on the environment?
- properties and evolution of the X-ray gas?
- do all elliptical galaxies contain a dead quasar?

7.2 Global Parameters

7.2.1 Stellar Density Profiles of Elliptical Galaxies

The stellar density profiles of elliptical galaxies differ from the profiles of disks or dwarf galaxies but are similar to those of massive bulges. The following profiles provide relatively good descriptions of the projected surface brightnesses:

● **King profiles (see Figure on following pages).** Quasi isothermal velocity distribution of stars but with a cut-off in energy. Stars have a minimum binding energy, the size of which determines the profile. High binding energy implies stronger concentration of the model (see Binney/Tremaine).

● $r^{1/4}$ -profile:

$$\Sigma(r) = \Sigma_e \cdot 10^{-3.33 \left[\left(\frac{r}{r_e} \right)^{1/4} - 1 \right]}$$

This is the most traditional model, r_e is the radius that contains half the projected light, Σ is the surface brightness, Σ_e the surface brightness at r_e .

 **Jaffe profile:**

$$\rho_L(r) = \frac{L}{4\pi r_0^3} \frac{1}{(r/r_0)^2} \frac{1}{(1 + r/r_0)^2}$$

L : total luminosity

ρ_L : luminosity density

$$\left. \begin{array}{l} r_e \text{ contains half of the } \underline{\text{projected light}} \\ r_0 \text{ contains half of the } \underline{\text{unprojected light}} \end{array} \right\} \Rightarrow r_e \simeq 0.76r_0$$

The Jaffe profile is most convenient, as it is fully analytic:

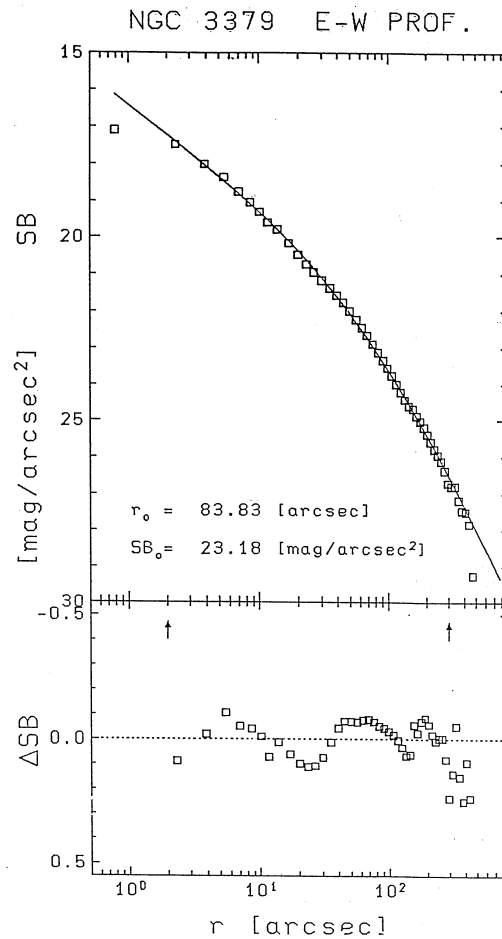
$$L(r) = L \frac{r}{r + r_0}$$

$$\Phi(r) = \frac{GL}{r_0} \left(\frac{M}{L} \right) \ln \frac{r}{r + r_0}$$

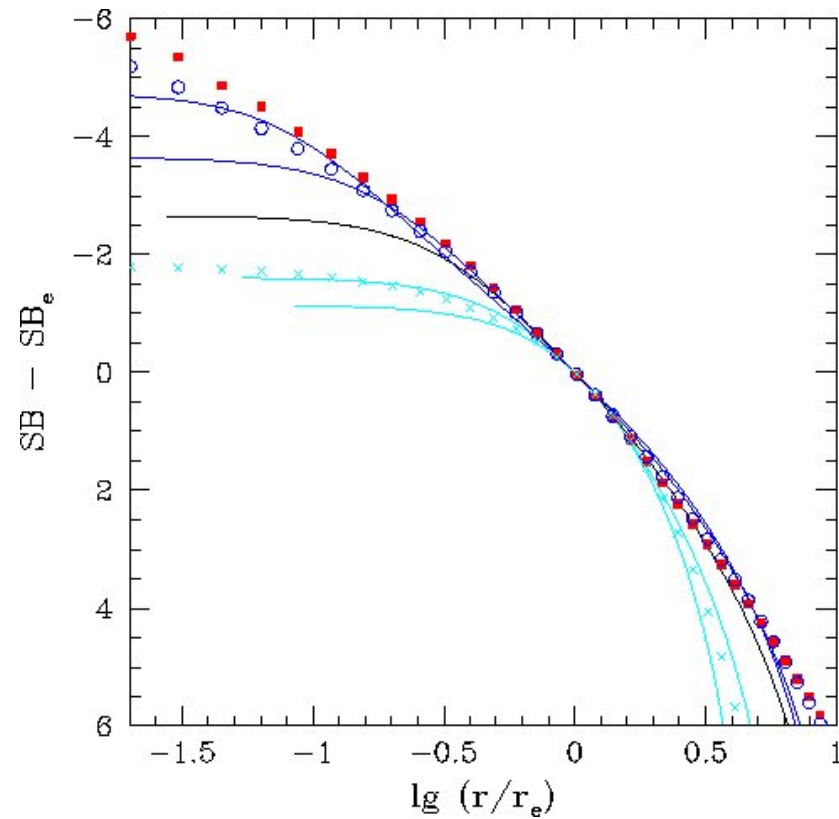
with the projected brightness distribution:

$$I(a) = \begin{cases} (4a)^{-1} + \frac{1}{2\pi}(1 - a^2)^{-1} - (1 - a^2)^{-3/2} \cdot (2 - a^2) \cdot \operatorname{arcosh} \left(\frac{1}{a} \right) & \text{for: } a < 1 \\ (4a)^{-1} - \frac{1}{2\pi}(a^2 - 1)^{-1} + (a^2 - 1)^{-3/2} \cdot (a^2 - 2) \cdot \arccos \left(\frac{1}{a} \right) & \text{for: } a \geq 1 \end{cases}$$

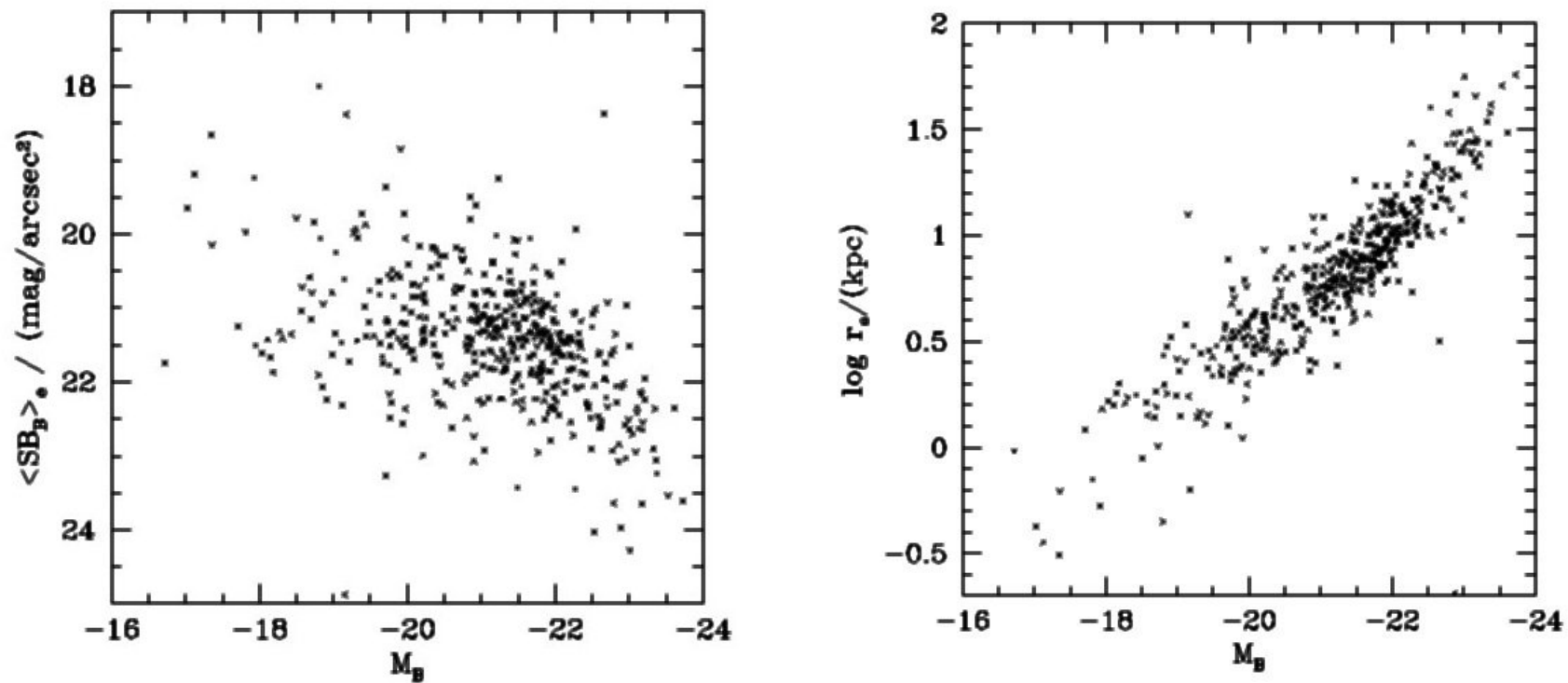
with $a = \frac{R}{r_0}$ and the projected distance from the center R .



Jaffe-fit to NGC 3379 from Surma, Seifert, Bender (1992) *A&A*



Comparison of different SB-profiles of galaxies.
 Red squares: Jaffe model, blue circles: $r^{1/4}$ -model, cyan crosses: exponential, lines
 are King models of different binding energy.



Effective radius r_e and mean effective surface brightness $\langle SB \rangle_e$ against M_B from Faber et al. survey (1989).

7.2.2 Density Profiles of the Core Regions of Elliptical Galaxies

- important for the dynamical structure (population of stellar orbits, see below)
- important for formation models (high density implies high collapse/dissipation with respect to the initial conditions)
- astonishingly strong correlation between core and global parameters exist (Kormendy 1985)
- **Key parameters for the description of galaxy cores:**

- core radius r_c :

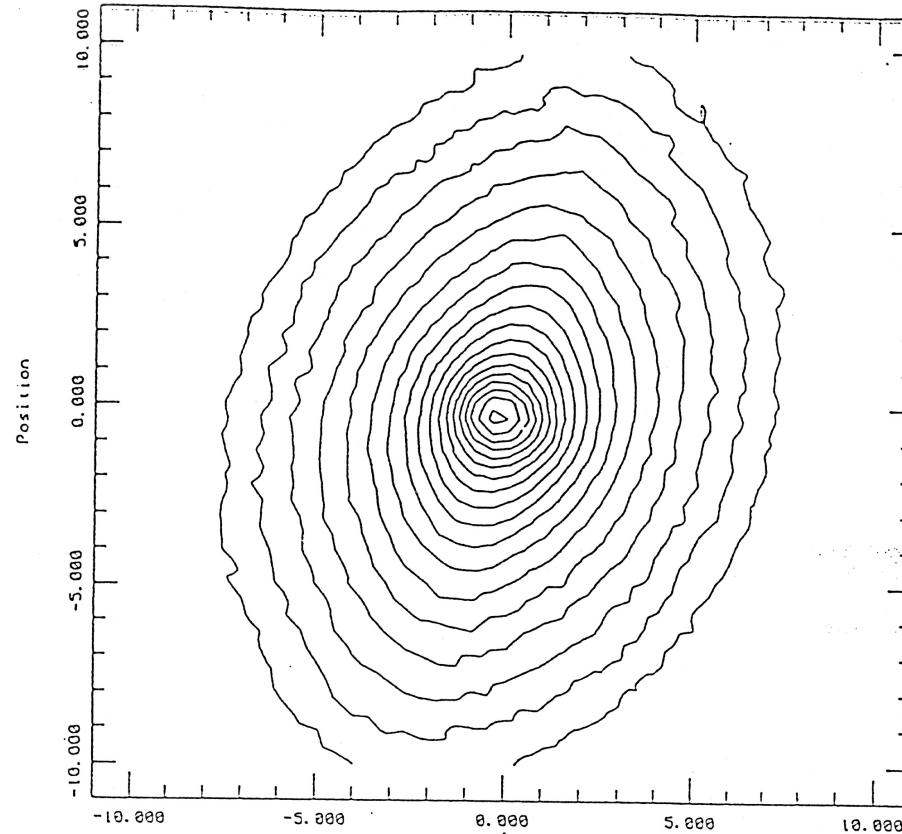
$$\Sigma(r_c) = \frac{1}{2}\Sigma(r = 0)$$

- central surface brightness:

$$\Sigma_0 = \Sigma(r = 0) \quad \text{or} \quad SB_0, \mu_0$$

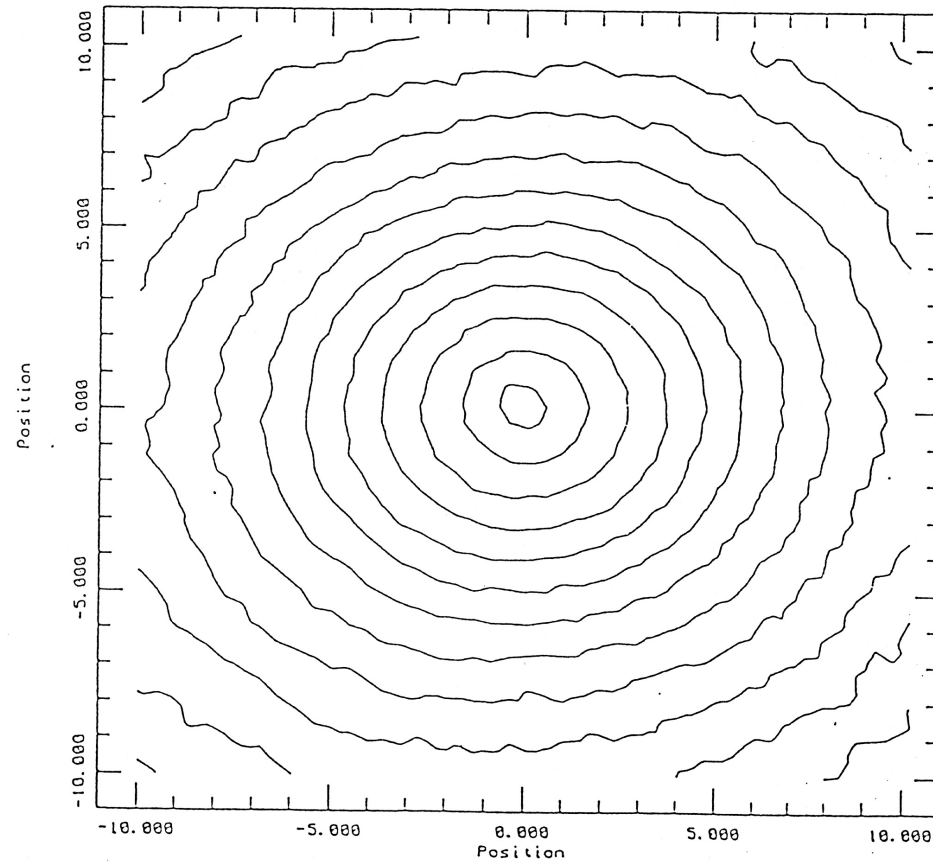
- central velocity dispersion:

$$\sigma_0 = \sigma(r = 0)$$



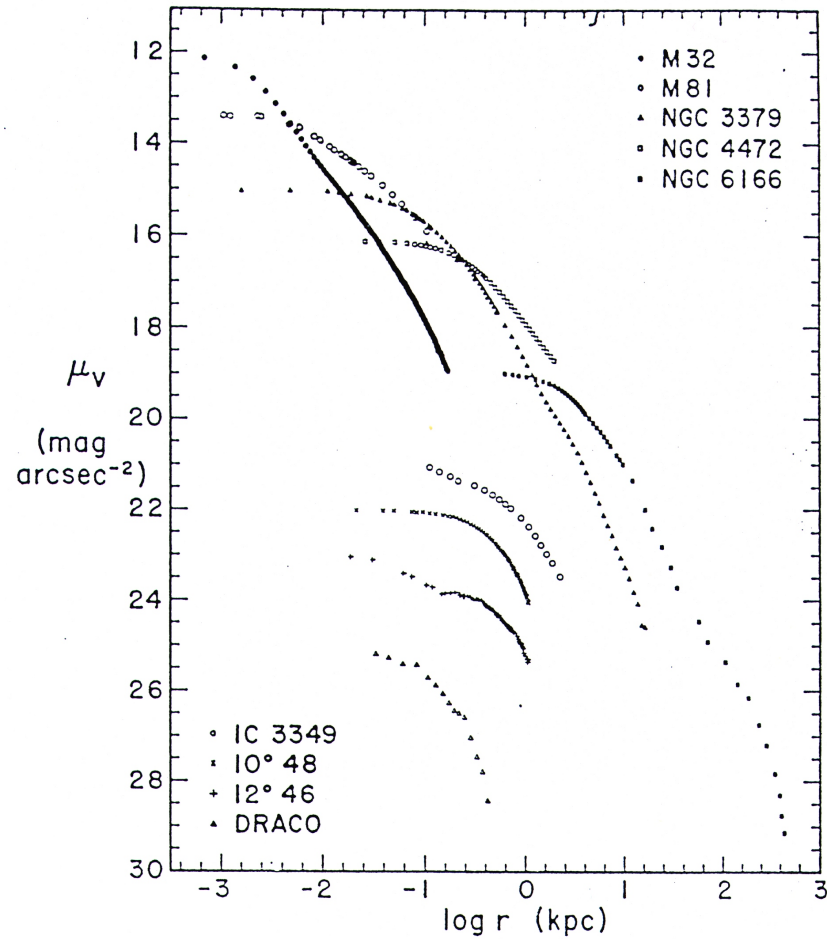
Central regions of the galaxy NGC 4621 out to radii of 10 arcsec.
The distance between the isophotes is 0.2 mag.

see: P. Surma (1988) *Diploma Thesis*



Central regions of the galaxy NGC 4649 out to radii of 10 arcsec.
The distance between the isophotes is 0.2 mag.

see: P. Surma (1988) *Diploma Thesis*



see: Kormendy (1985)

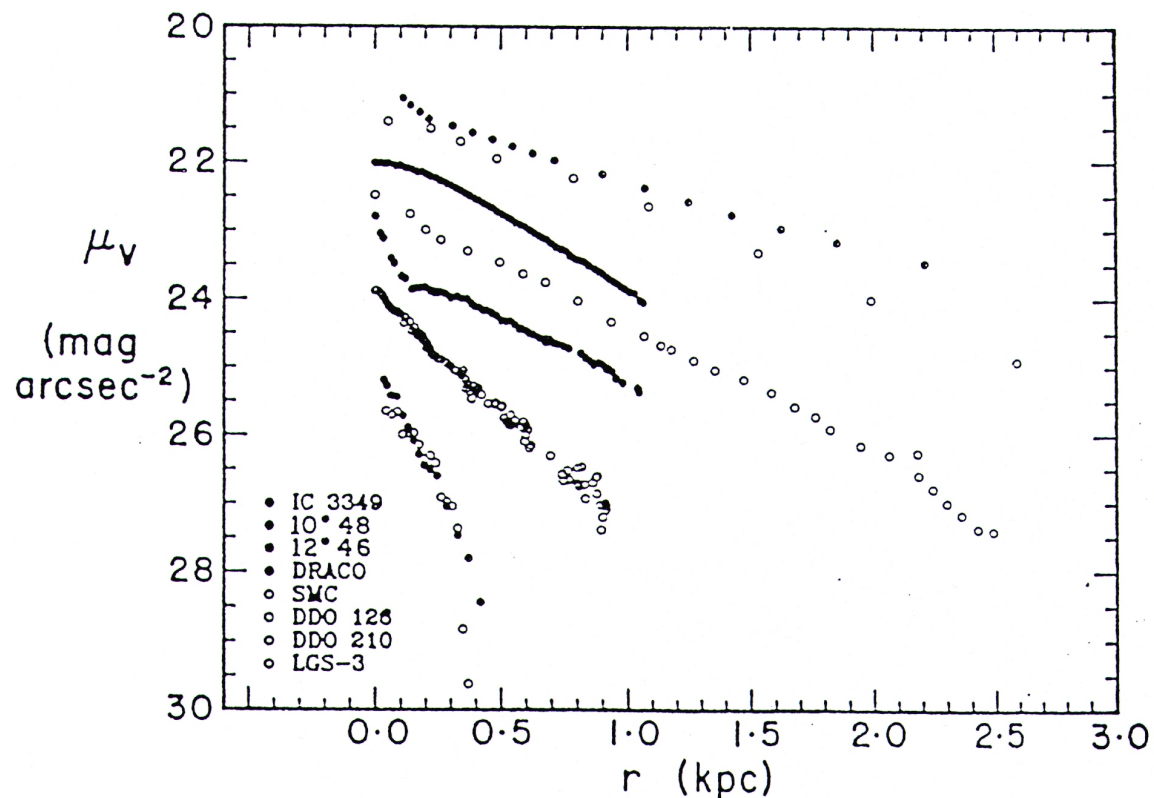
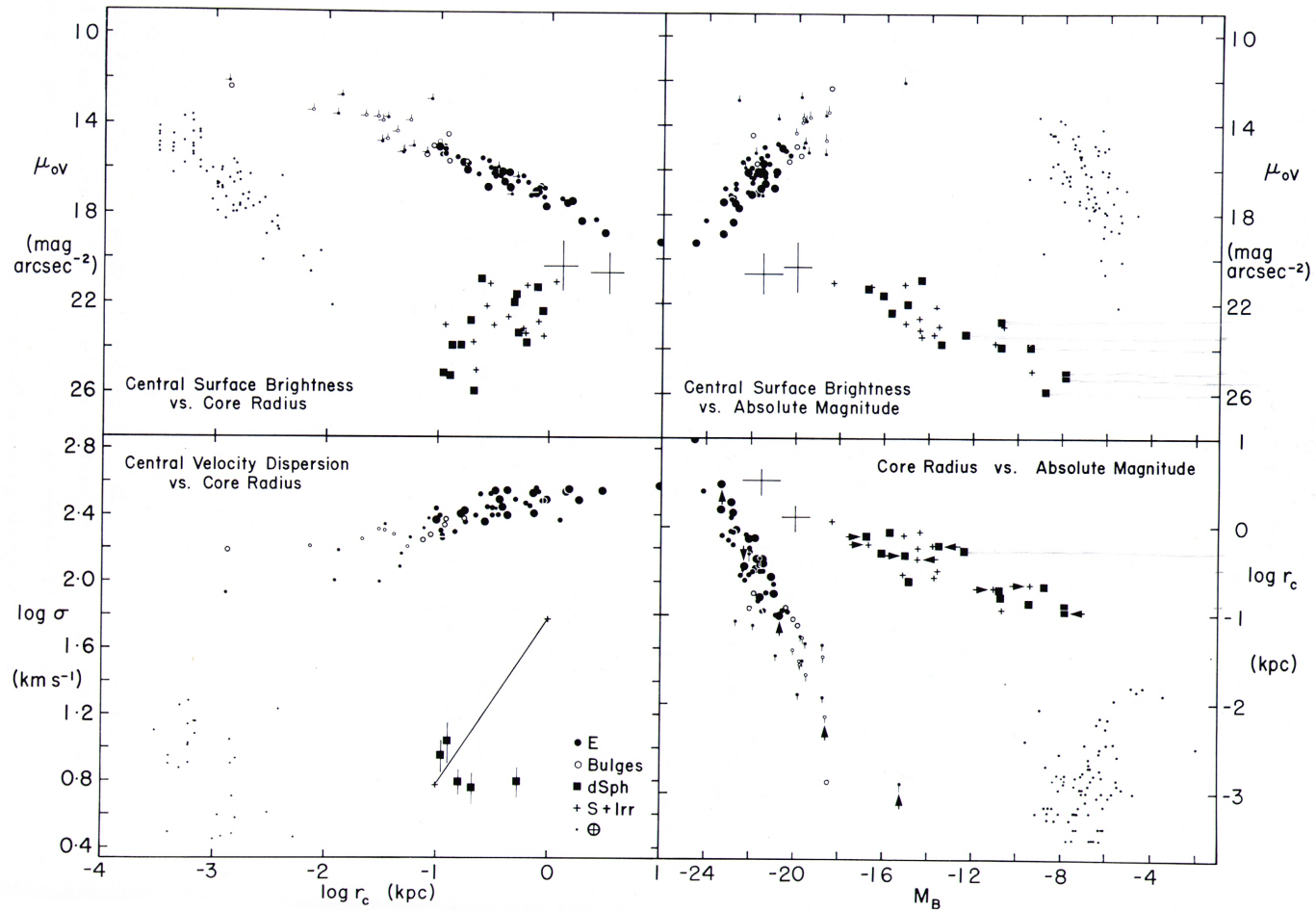


Fig. 4. - (a, top) Mean brightness profiles of fiducial galaxies along the E and dSph sequences. (b, bottom) Brightness profiles of fiducial dSph and dS+I galaxies. The galaxies are identified by arrows in Fig. 2.

see: Kormendy (1985)



see: Kormendy (1987) *Nearly Normal Galaxies*, Springer Verlag

● if the core region is **isothermal**, i.e the stellar velocity dispersion is approximately isotropic and radially constant, then one can derive on the basis of the King models:

● **density:**

$$\rho_0 \simeq \frac{\Sigma_0}{2r_c}$$

● **mass-to-light ratio:**

$$\frac{M}{L} \simeq \frac{9\sigma_0^2}{2\pi G \Sigma_0 r_c}$$

in the past, this formula was used to estimate M/L . Today, complete models for the whole galaxies (not just the cores) are constructed to derive more reliable M/L .

NGC	$-M_B$	$\frac{\sigma}{km.s^{-1}}$	Υ_V	NGC	$-M_B$	$\frac{\sigma}{km.s^{-1}}$	Υ_V
720	19.9	240	10	4406	20.6	262	12
741	21.2	309	18	4472	21.3	317	13
1395	19.5	245	16	4552	19.9	276	11
1407	20.0	288	22	4636	20.1	227	16
1600	21.1	342	19	4649	20.8	361	18
3379	19.4	227	10	5846	20.4	255	18
4261	20.8	321	13	6086	21.1	331	15
4365	20.0	263	16	7619	20.6	304	12
4374	20.4	292	11	7626	20.5	275	16

Velocity dispersions and mass-to-light ratios Υ_V of some elliptical galaxies, using a Hubble constant $H_0 = 100 km s^{-1} Mpc^{-1}$. The mass-to-light ratios are derived from the virial theorem for brightness profiles similar to King profiles (see Binney/Tremaine).

7.3 Isophotes and the Shape of Elliptical Galaxies

7.3.1 Three-Dimensional Shape

- Isophotes are in the first order elliptical
 \Rightarrow the density is constant in ellipsoids,
 i.e. the possible shapes are:

oblate ($a = b > c$, like a flying saucer)

prolate ($a > b = c$, like a cigar)

triaxial ($a \neq b \neq c$, like a box with smoothed edges)

- Projection for the axially symmetric case (oblate or prolate):

$$q_{int}^2 \sin^2 i + \cos^2 i = \begin{cases} q_{proj}^2 & \text{(oblate)} \\ 1/q_{proj}^2 & \text{(prolate)} \end{cases}$$

with $q = \frac{\text{minor axis}}{\text{major axis}} = \frac{b}{a}$,

and i : angle between the c-axis and the line of sight

(see: Binney/Merrifield)

- Projection for the triaxial case:
Evidently more complicated (see: Ryden (1990) *ApJ*)
- From the observed projected ellipticity distribution (as well as from kinematic measurements) one can estimate that elliptical galaxies are in the mean modestly triaxial (near oblate): $a : b : c \simeq 1 : 0.95 : 0.7$
- An important side effect of a triaxial density distribution is the so-called **isophote twist** which is observed in many ellipticals.

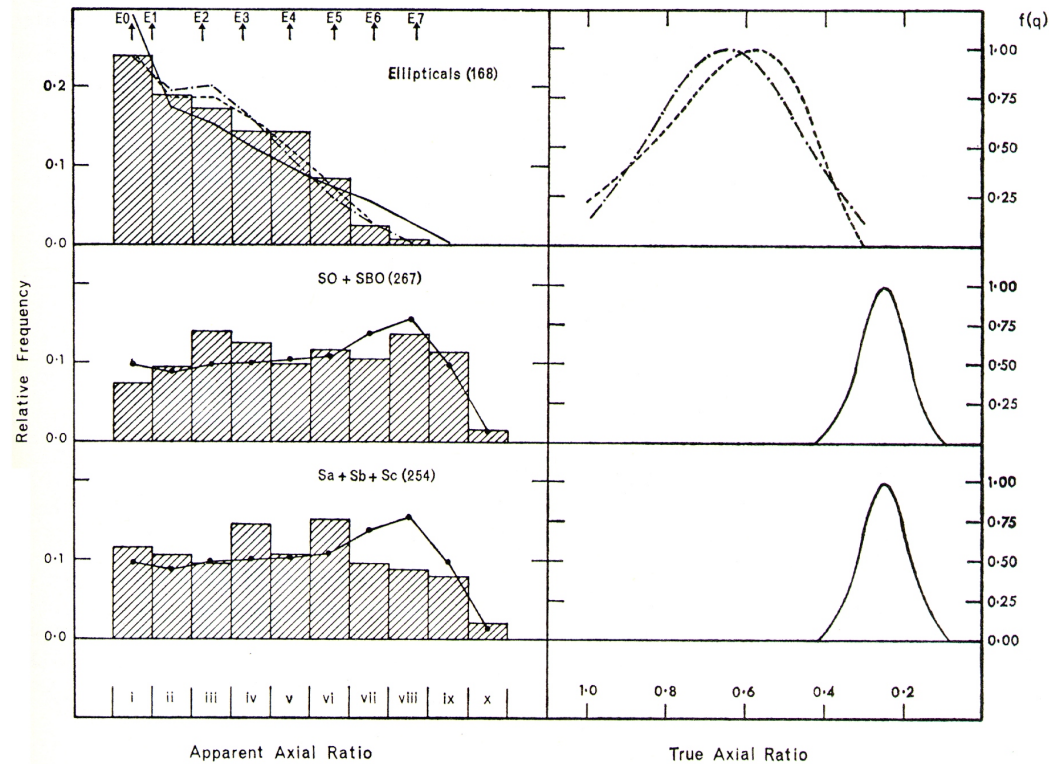


FIG. 1.—*Left*, histograms of the distribution of apparent axial ratios for E, S0, and spiral galaxies, sorted into class intervals defined in Tables 1 and 2. The curves are predicted ratios for various assumptions of the distribution of intrinsic flattening. *Right*, assumed intrinsic distributions corresponding to the curves on the left. The case of uniform flattening for E galaxies is a straight horizontal line truncated at $b/a = 0.3$ and is not shown. Dot-dash curve is a Gaussian with $q_0 = 0.65$ and $\sigma = 0.18$. Dashed curve is a skewed binomial distribution defined in the text, with $q_0 = 0.58$, $a = 0.31$, and $p = 3.0$. The two solid curves are Gaussians with $q_0 = 0.25$ and $\sigma = 0.06$.

see: Sandage A. et al. (1970) *ApJ*, **160**, 831

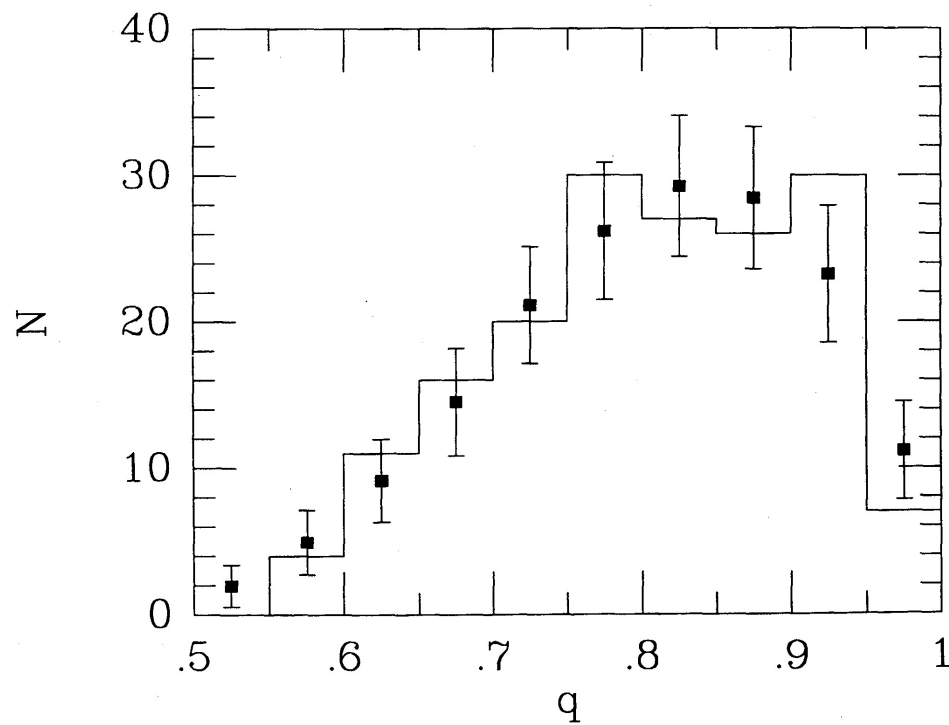


FIG. 6.—Binned distribution functions of apparent axis ratios. The histogram gives the apparent axis ratios of the 171 elliptical galaxies in the observational sample. The points and error bars give the mean and standard deviation expected from a sample of 171 galaxies drawn from the Gaussian function $f(\beta, \gamma)$ with $\sigma_0 = 0.11$, $\beta_0 = 0.98$, and $\gamma_0 = 0.69$. The two functions have a reduced χ^2 score of $\chi^2/\nu = 1.2$.

see: Ryden (1992) *ApJ*, **396**, 445R

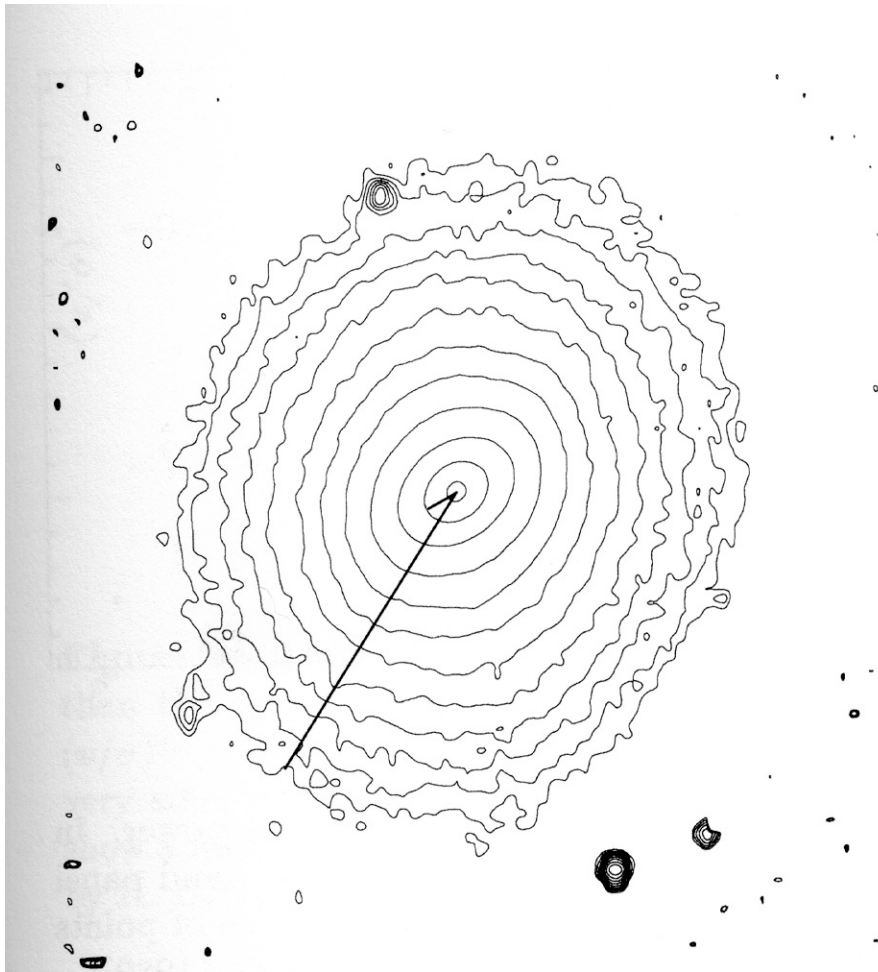


Figure 4.37 Isophotes (at $0.5 \mu_r$ intervals) of the E3 galaxy, NGC 5831. The heavier lines indicate the semi-major axes of the ellipses that best fit the isophotes at two radii. These axes have lengths $a = 4$ arcsec and $a = 40$ arcsec. [From data kindly provided by R. Bender]

see: Binney/Merrifield *Galactic Astronomy*

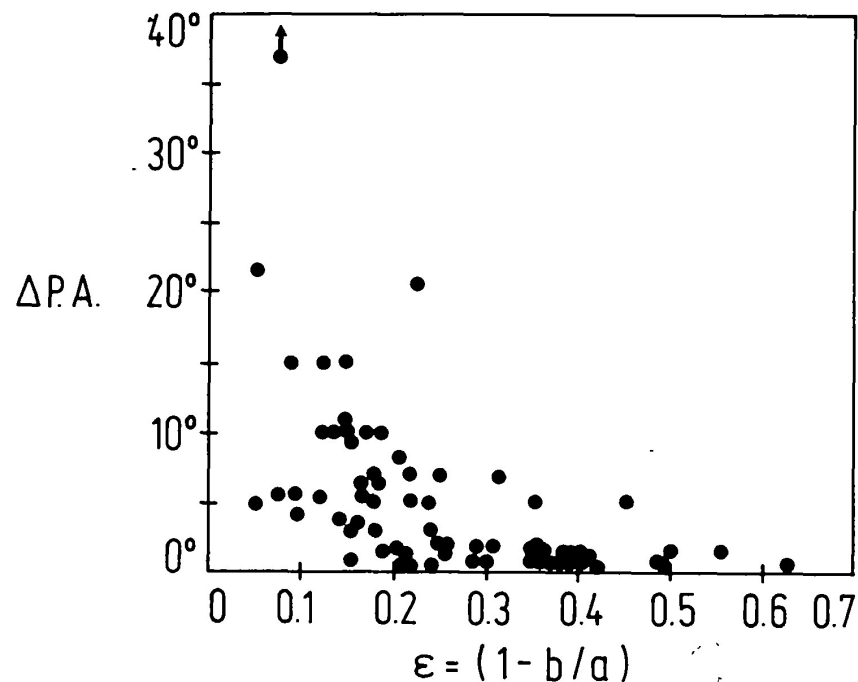


FIGURE 9. — The isophote twists between the innermost isophote not affected by seeing or guiding errors and $1.5 r_e$ ($r_e =$ de Vaucouleurs radius) as a function of the ellipticities for all galaxies observed.

see: Bender R. et al. (1988) *A&AS* **74**, 385B

7.3.2 Shape of the Isophototes of Elliptical Galaxies

Deviations from elliptical isophotes:

Isophotes are generally not exactly elliptical. The “**boxiness**” or “**diskiness**” of isophotes is usually quantified by measuring a quantity denoted a_4 . First the ellipse $R_e(\varphi)$ is fitted to the isophote. Then for each angle φ one determines the distance $\delta(\varphi) = R_i(\varphi) - R_e(\varphi)$ between the radii of corresponding points on the ellipse and on the isophote. Then one expresses the function $\delta(\varphi)$ as a Fourier series:

$$\delta(\varphi) = \bar{\delta} + \sum_{n=1}^{\infty} a_n \cos(n\varphi) + \sum_{n=1}^{\infty} b_n \sin(n\varphi)$$

a_4 is the smallest deviation of the isophote relative to the ellipse, that is dynamically plausible.

$a_4 < 0$: boxy isophotes $a_4 > 0$: disky isophotes

FIGURE 3. — Distribution of the ellipticity classes for all observed elliptical galaxies.

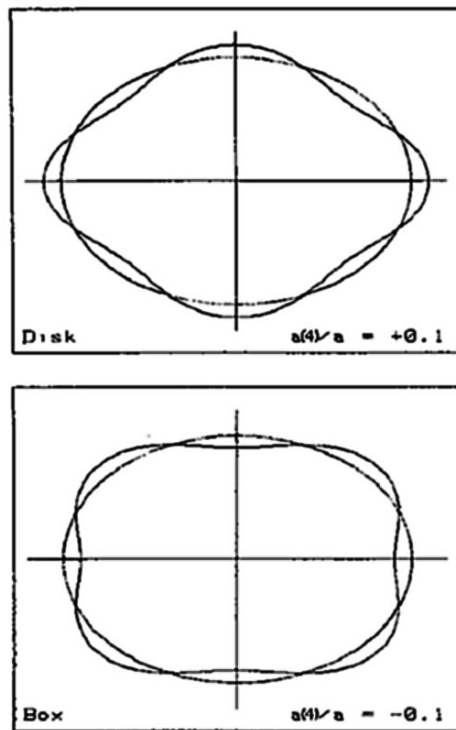


FIGURE 5. — Schematic drawing illustrating isophotes with $a(4)/a = +0.1$ and $a(4)/a = -0.1$.

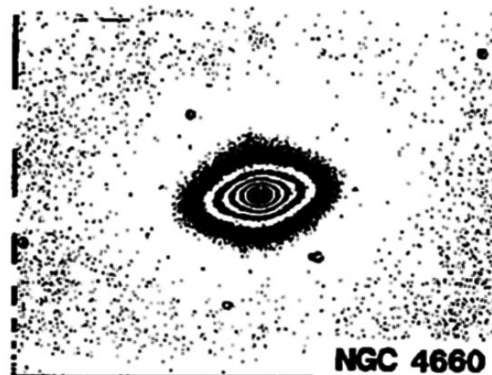


FIGURE 6. — R-image of NGC 4660, an elliptical galaxy with a disk-component in the isophotes ($a(4)/a \sim +0.03$).



FIGURE 7. — R-image of NGC 5322, an elliptical galaxy with box-shaped isophotes ($a(4)/a \sim -0.01$).

Examples for boxy and disky isophotes from Bender et al. (1988)

Disky isophotes can be explained by a superposition of an elliptical bulge and a faint edge-on disk. Isophote shape analysis is perhaps the only possibility to detect weak disks in ellipticals.

Are disky Es related to S0s? Are they forming an intermediate type between boxy Es and S0s? The answer is probably yes. The properties of the disks in terms of radii and densities smoothly overlap with those of S0 galaxies.

7.4 Dynamics and Kinematics

7.4.1 Stellar Dynamics of Elliptical Galaxies

- A great variety of stellar orbits can be found in elliptical galaxies. Main types are:
 - **box orbits**
 - **short axis tubes**
 - **long axis tubes**

The envelopes of these three orbit families are given on the next pages.

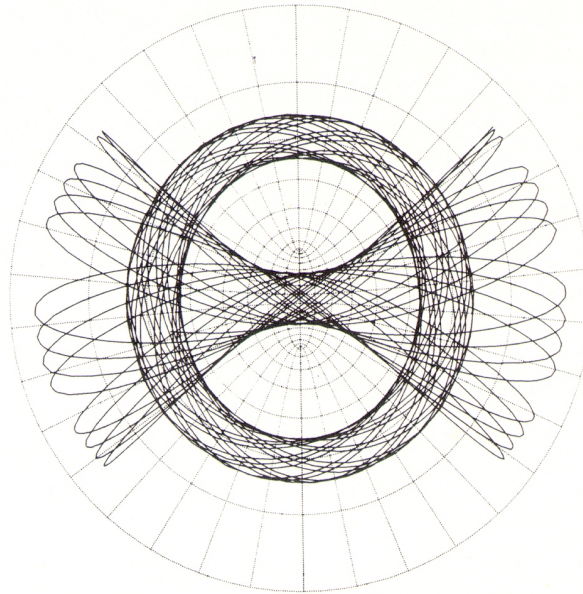


Figure 3-21. The boundaries of loop and box orbits in barred potentials approximately coincide with the coordinate curves of a system of spheroidal coordinates. The figure shows two orbits in the potential Φ_L of equation (3-77), and a number of curves on which the coordinates u and v defined by equations (3-130) are constant.

Stellar Orbits in a two-dimensional barred potential (Binney/Tremaine)

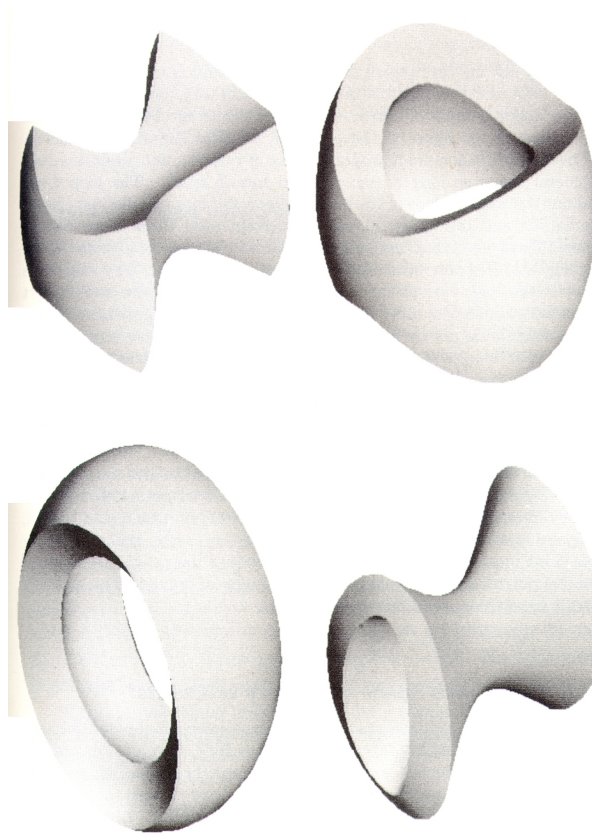


Figure 3-20. Orbits in a nonrotating triaxial potential. Clockwise from top left: (a) box orbit; (b) short-axis tube orbit; (c) inner long-axis tube orbit; (d) outer long-axis tube orbit. [Courtesy of T. Statler; see Statler (1986).]

Stellar Orbits in a triaxial potential (Binney/Tremaine)

- In order to determine the kinematics of an elliptical galaxy one needs to derive velocities, velocity dispersions (and possibly higher moments) along each line of sight. Since the spectra of ellipticals are broadened by velocity dispersion, the absorption lines of the spectra overlap and it is not possible to derive the kinematics from the analysis of single absorption lines. Therefore, more sophisticated methods are needed.
- For example, v and σ can be measured by deconvolution of the galaxy spectrum $G(\lambda)$ with a spectrum $S(\lambda)$ of a suitable comparison star (e.g. K0III star). For each line-of-sight through the galaxy one approximately has

$$G(\lambda) = g(\lambda) \otimes B(v, \sigma, \dots)$$

with:

G = galaxy spectrum as observed,

g = mean spectrum of all stars along the line of sight without relative motion,

B = velocity distribution along the line of sight

- An approximate determination of $B(v, \sigma, \dots)$ is obtained by division in Fourier space with a template star $S(\lambda)$:

$$\tilde{B}(v, \sigma) \simeq \frac{\tilde{G}}{\tilde{S}} = \tilde{B}(v, \sigma, \dots) \cdot \frac{\tilde{g}}{\tilde{S}}$$

If the template star is chosen properly, then:

$$\frac{\tilde{g}}{\tilde{S}} \simeq 1$$

$\Rightarrow v, \sigma$ can be determined by fitting a Gaussian function to $\frac{\tilde{G}}{\tilde{S}}$.

● This is the classical way to determine v, σ :

Fourier Quotient Method (Sargent et al. (1978))

● Nowadays improved methods are used, that are more robust against differences between \tilde{g} and \tilde{S} :

● Fourier Correlation Quotient Method (Bender (1990))

● Spectral Fitting Method (Rix and White (1992))

● Fourier Fitting Method (Franx and v.d. Marel (1993))

These new methods also allow the determination of deviations of the line-of-sight velocity distributions from Gaussians.

Typical Rotation and Dispersion Curve for an Elliptical Galaxie:

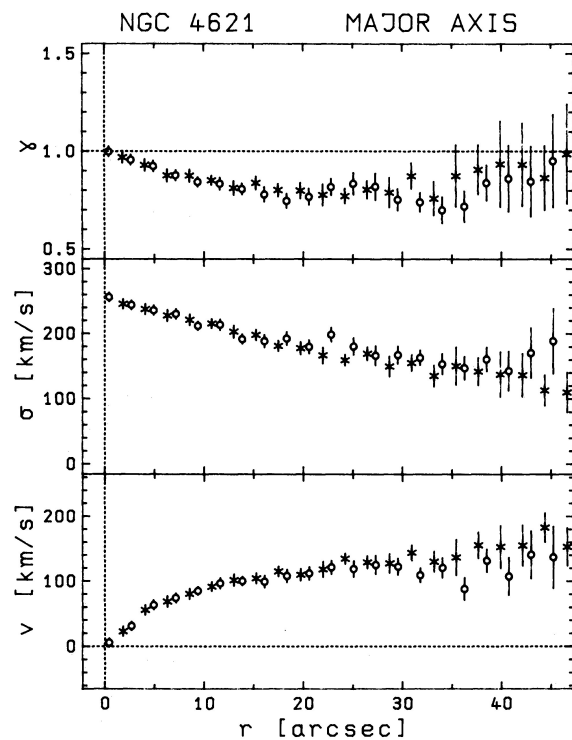
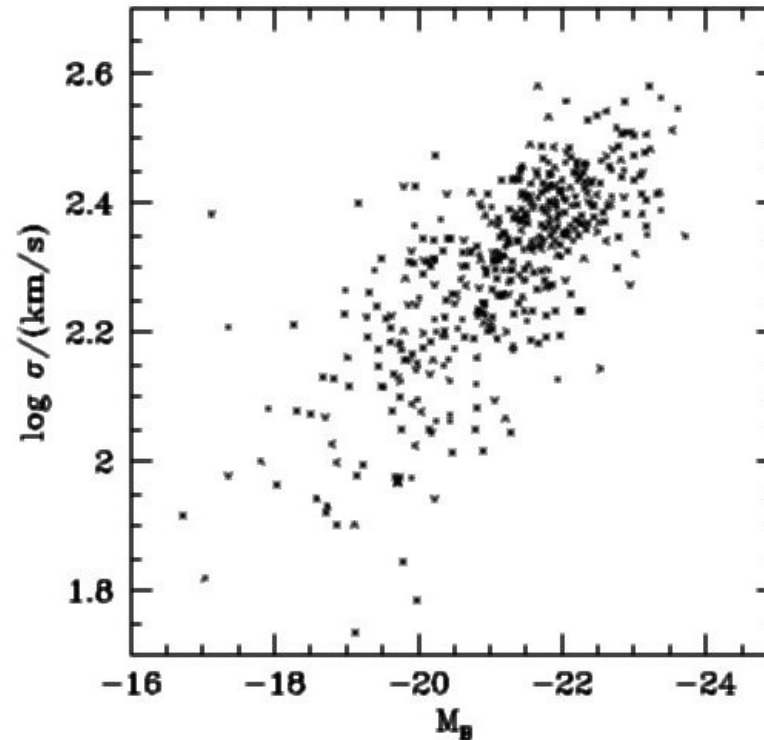


Fig. 7. Rotation velocity v , velocity dispersion σ and line strength γ along the major axis of NGC 4621 as a function of the radius r . The curves were folded about the nucleus; different sides are represented by different symbols.

see: Bender (1990) *A&A*, **229**, 441



Faber-Jackson relation between central velocity dispersion and total magnitude of elliptical galaxies

$$L_B \propto \sigma^4$$

7.4.2 Flattening of Elliptical Galaxies and Bulges – An application of the Tensor Virial Theorem

Consider a stable ($\frac{d^2I}{dt^2} = 0$) axisymmetric elliptical with the z -axis being the axis of symmetry, then one has:

$$\Rightarrow \left\{ \begin{array}{l} W_{xx} = W_{yy} \ ; \ W_{ij} = 0 \ \text{for } i \neq j \\ \Pi_{xx} = \Pi_{yy} \ ; \ \Pi_{ij} = 0 \ \text{for } i \neq j \\ T_{xx} = T_{yy} \ ; \ T_{ij} = 0 \ \text{for } i \neq j \end{array} \right\}$$

The only remaining non-trivial Tensor Virial Equations are:

$$2T_{xx} + \Pi_{xx} + W_{xx} = 0 \quad ; \quad 2T_{zz} + \Pi_{zz} + W_{zz} = 0$$

or:

$$\boxed{\frac{2T_{xx} + \Pi_{xx}}{2T_{zz} + \Pi_{zz}} = \frac{W_{xx}}{W_{zz}} \simeq \left(\frac{a}{b}\right)^{0.89}}$$

with

$$\left. \begin{array}{l} a = \text{major axis} \\ b = \text{minor axis} \end{array} \right\} \text{ of the rotation ellipsoid}$$

Note: The approximation for $\frac{W_{xx}}{W_{zz}}$ for rotation ellipsoids does not depend on their density profiles (see Binney/Tremaine)!

1. Rotational flattening: $\Pi_{xx} = \Pi_{yy} = \Pi_{zz} = M\sigma_0^2$

with the mass-weighted mean-square random velocity along the line of sight to the galaxy σ_0^2

Using:

$$T_{xx} + T_{yy} = \frac{1}{2} \int \rho \bar{v}_\phi^2 d^3x = \frac{1}{2} M v_0^2; \quad T_{zz} = 0$$

with the mass-weighted mean-square rotation speed v_0^2 leads to:

$$\frac{v_0}{\sigma_0} \simeq \sqrt{2 \left(\frac{a}{b}\right)^{0.89} - 2} \simeq \frac{4}{\pi} \sqrt{\frac{1 - b/a}{b/a}}$$

Note: σ_0 and v_0 are not observed, but:

$$\left. \begin{array}{l} v_m = \text{typical rotation velocity} \\ \bar{\sigma} = \text{mean } \sigma \text{ within } \frac{r_e}{2} \end{array} \right\} \Rightarrow \frac{v_m}{\bar{\sigma}} \simeq \frac{\pi v_0}{4 \sigma_0}$$

E.g.

$$\frac{b}{a} = 0.7 \Rightarrow \frac{v_0}{\sigma_0} \simeq 0.8$$

2. Flattening by anisotropy: $T_{xx} = T_{yy} = T_{zz} = 0$

With $\Pi_{xx} = M\sigma_x^2$; $\Pi_{zz} = M\sigma_z^2$ follows:

$$\frac{\sigma_z}{\sigma_x} \simeq \left(\frac{b}{a}\right)^{0.45}$$

E.g.:

$$\frac{b}{a} = 0.7 \Rightarrow \frac{\sigma_z}{\sigma_x} \simeq 0.87$$

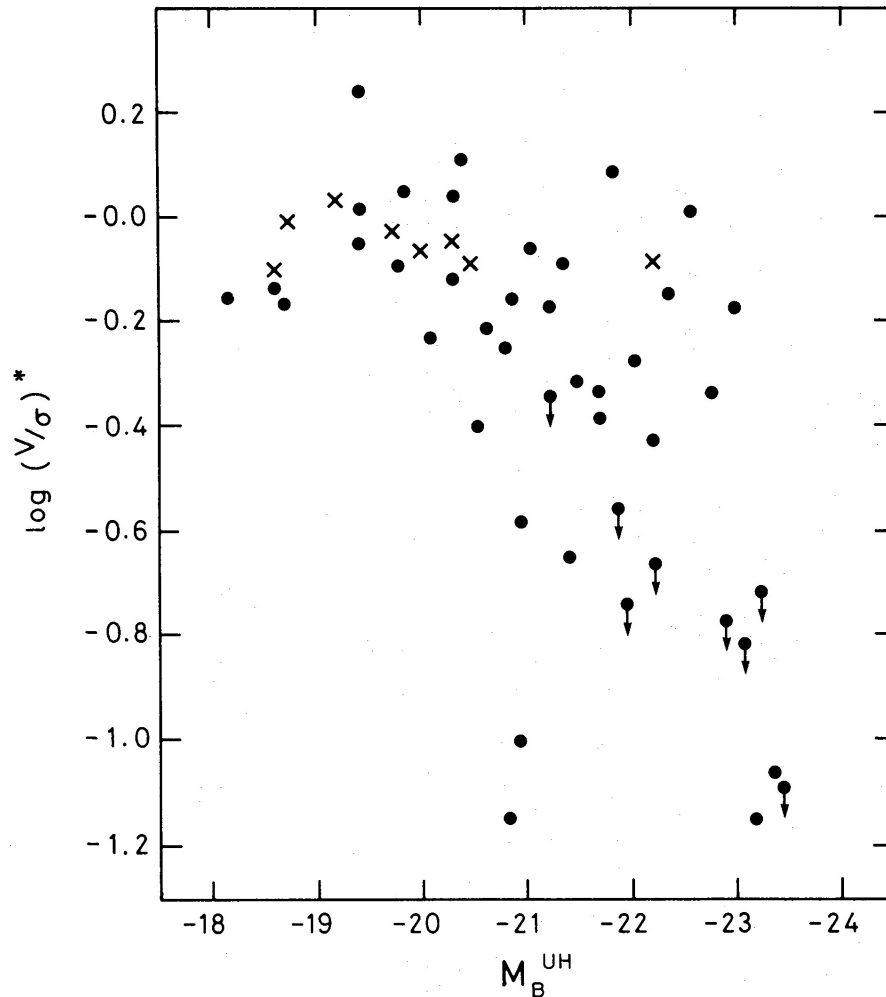


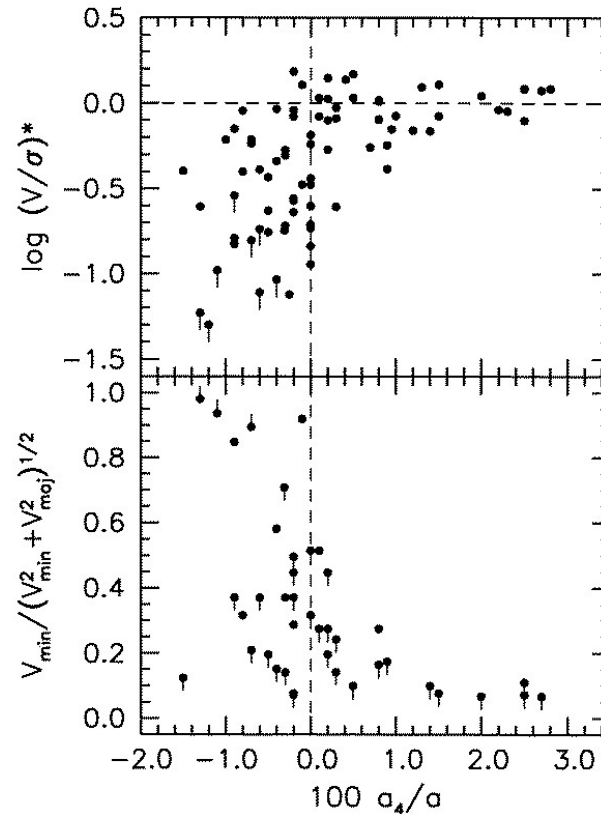
FIG. 4.— $\log (V/\sigma)^*$ against absolute magnitude. Ellipticals are shown as filled circles and the bulges as crosses; $(V/\sigma)^*$ is defined in § IIIb.

Rotational Properties of Elliptical Galaxies:

Anisotropy parameter:

$$\left(\frac{v}{\sigma}\right)^* \equiv \frac{v/\sigma}{\sqrt{\frac{1-b/a}{b/a}}} = \frac{(v/\sigma)_{\text{observed}}}{(v/\sigma)_{\text{rot. flattened}}}$$

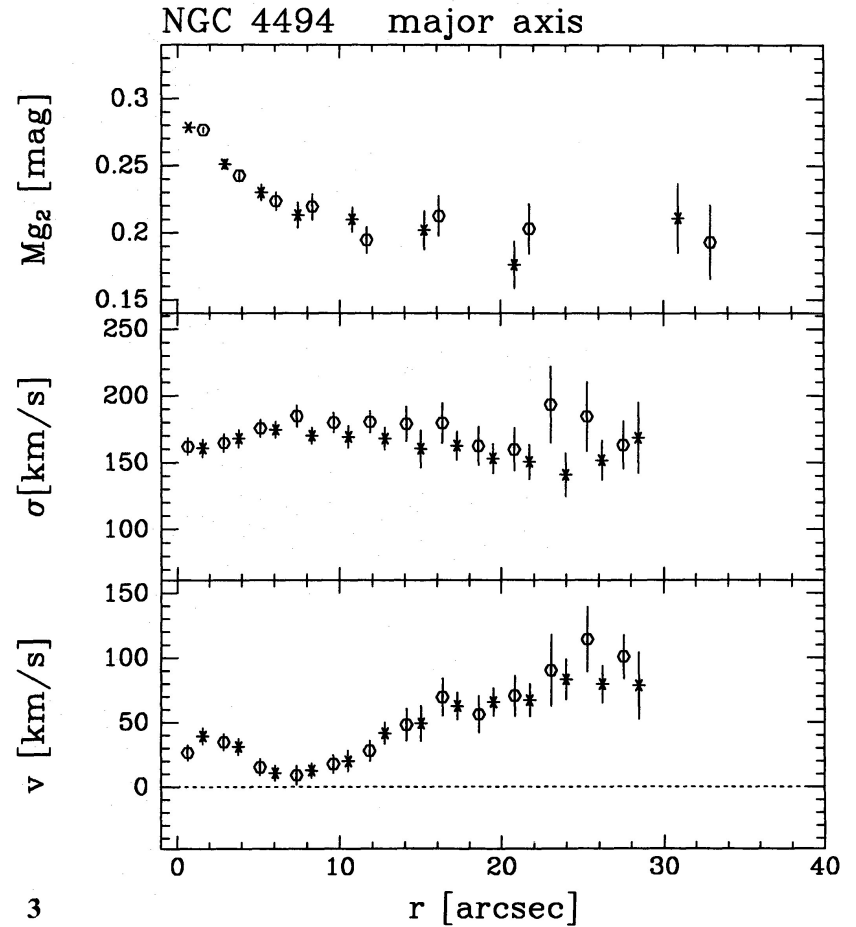
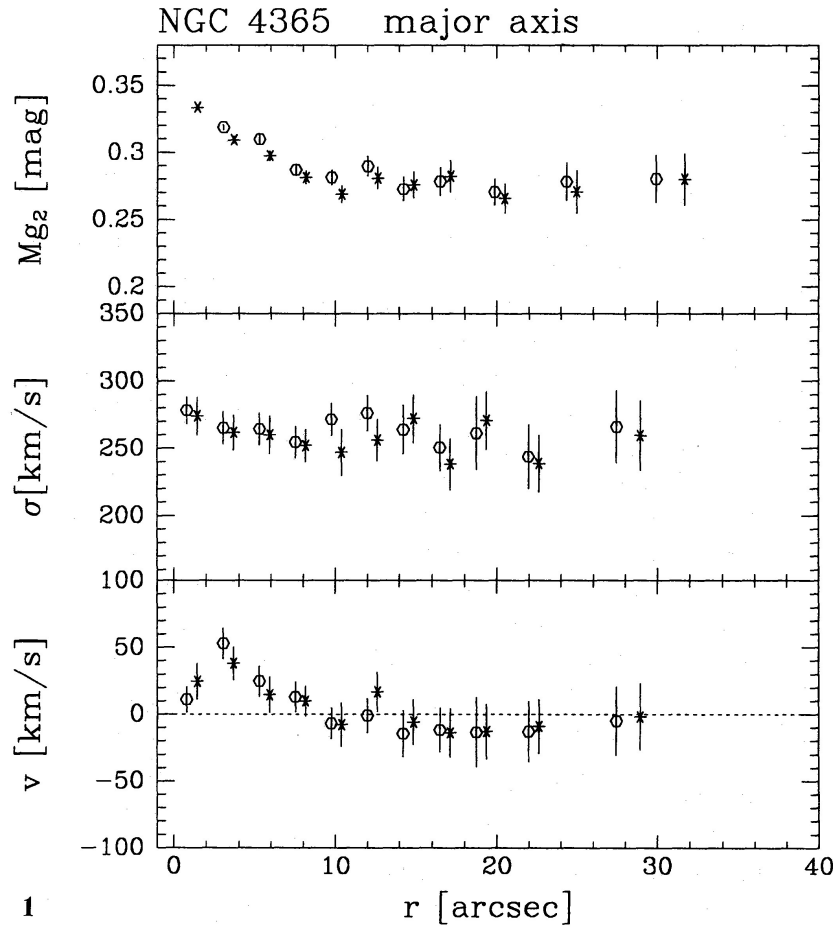
see: Davies et al. (1983)
ApJ, **266**, 41



Anisotropy correlates well with a_4/a , better than with luminosity. This confirms the continuity between disky ellipticals and S0 galaxies. Boxy ellipticals also show minor axis rotation, indicative of triaxiality, see Bender (1988), Kormendy and Bender (1996)

7.4.3 Counter-Rotating Nuclei

- Evidence for inhomogeneous collapse or merging process.
- Counter-rotation extends radially much farther than the core radius r_c .
(Up to $5r_c$)
- Counter-rotating and peculiar nuclei are much more metal rich than the rest of the galaxy.



see: Bender (1992) *A&A*, **258**, 250

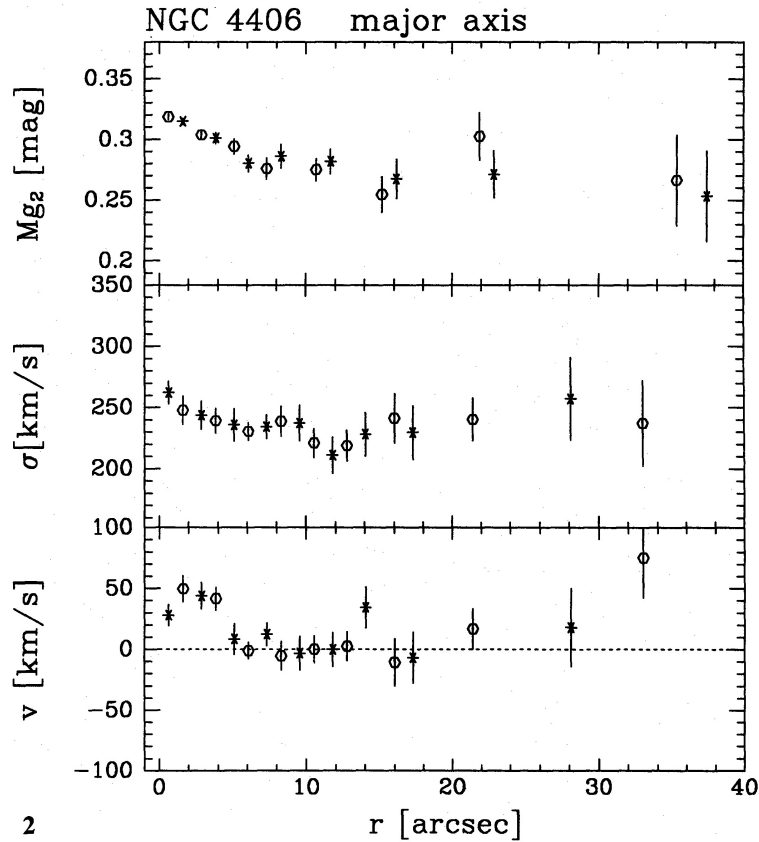


Fig. 1 and 2. Rotation velocity v , dispersion σ and Mg_2 -index against linear major axis radius r in NGC 4365 and NGC 4406. Different symbols refer to different sides from the center of the galaxy

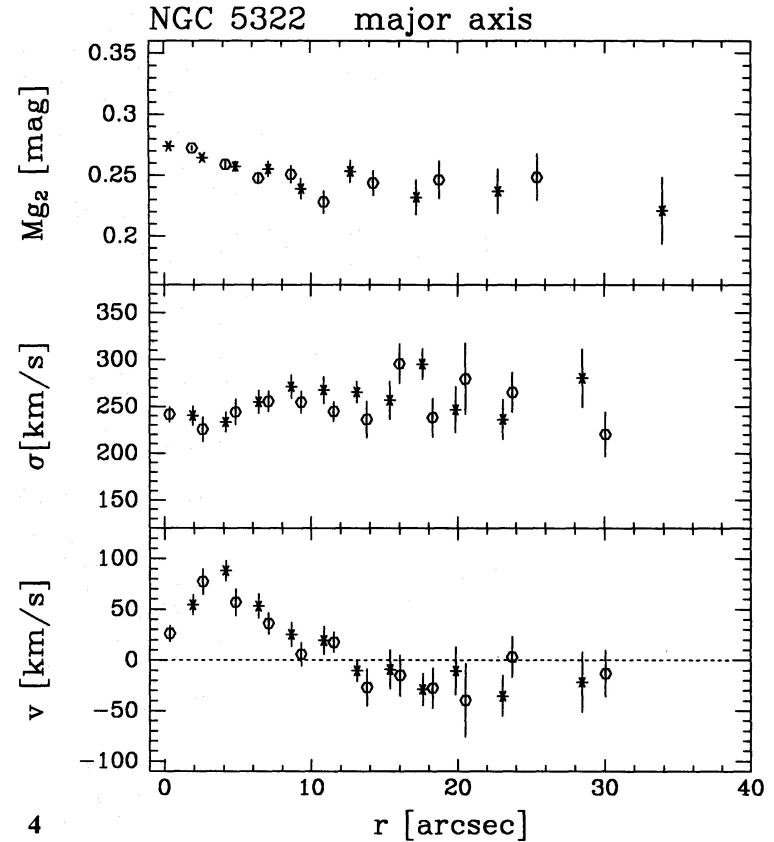


Fig. 3 and 4. Rotation velocity v , dispersion σ and Mg_2 -index against linear major axis radius r in NGC 4494 and NGC 5322. Different symbols refer to different sides from the center of the galaxy

see: Bender (1992) *A&A*, **258**, 250

7.4.4 Results of the Kinematics of Elliptical Galaxies

- Faint ellipticals and bulges are rotationally flattened, bright ellipticals are often anisotropic
- Strong correlation between rotational properties and the shape of the isophotes:
boxy isophotes: anisotropic, peculiar velocity fields
disky isophotes: usually rotationally flattened
- Counter-rotating nuclei show, that ellipticals cannot be formed by the collapse of uniformly rotating gas spheres. (→ formation by merging processes?)
- High rotation velocities and high dispersion in the core regions of some nearby E and S0 galaxies indicate the existence of massive black holes ($M \sim 10^6 \dots 10^8 M_{\odot}$)

7.5 Mass-to-Light Ratios

The mass-luminosity ratios for the central regions of elliptical galaxies can be determined similar to the dwarf elliptical galaxies using the virial theorem or from analysis of the core properties (see above):

⇒ There is no evidence for dark matter dominating in the central regions of elliptical galaxies:

$$\boxed{\frac{M}{L} \propto 10 \frac{M_{\odot}}{L_{B,\odot}}}$$

But: the stellar density in E galaxies is much higher than in dwarf galaxies, so that even $\rho_{\text{DM}} \propto 1 \frac{M_{\odot}}{\text{pc}^3}$ is not detectable!

⇒ Main question: Does dark matter dominate at large radii as in spirals?